Communication

Interlaced Fourier transformation of ultrafast 2D NMR data

Mor Mishkovsky, Lucio Frydman*

Department of Chemical Physics, Weizmann Institute of Science, 76100 Rehovot, Israel

Received 14 December 2004; revised 24 December 2004

Abstract

A new protocol for processing the data arising in ultrafast 2D NMR is discussed and exemplified, based on the interlaced Fourier transformation. This approach is capable of dealing in a single, combined fashion, with the two mirror-imaged interferograms arising in this kind of experiment as a result of the acquisition of a train of magnetic field gradient echoes. By combining all the acquired data points into a common Fourier processing procedure the spectral width along the direct-acquisition domain becomes effectively doubled, giving the opportunity of employing acquisition gradients that are approximately half as strong as hitherto required. This in turn should lead to an overall enhancement in the signal-to-noise ratio of the experiment of ca. 2, as well as to improvements in the achievable digital resolution. These expectations were tested by carrying out a series of homo- and heteronuclear ultrafast 2D NMR acquisitions, and found systematically fulfilled. The robustness and conditions that allow the interlaced numerical procedure to be implemented in routine analytical applications were explored and are briefly discussed.
© 2005 Elsevier Inc. All rights reserved.

Keywords: Ultrafast 2D NMR; Interlaced Fourier transformation; Signal-to-noise ratio; Sensitivity enhancement; Spectral resolution

Two-dimensional spectroscopy constitutes one of the cornerstones underlying the analytical applications of nuclear magnetic resonance (NMR). In a traditional 2D NMR experiment [1,2] data are collected as a function of two variables: a physical acquisition time t_2 encoding the direct-domain frequencies Ω_2, and an evolution time t_1 encoding the pre-mixing frequencies Ω_1. As this latter time is actually a parameter within the NMR pulse sequence, monitoring its effects requires the collection of several independent scans whereby t_1 values are systematically incremented [1–4]. This in turn makes high-dimensional NMR experiments inherently more time consuming than their unidimensional counterparts. Recently, an alternative "ultrafast" approach has been proposed that departs from this sampling mode, and enables the acquisition of 2D—and in general of nD—NMR spectra within a single scan [5–7].

In its most common implementation ultrafast 2D NMR replaces the t_1 encoding involved in traditional 2D spectroscopy, with an analogous gradient-assisted encoding of the spin interactions along an arbitrary geometry. The winding of spin coherences associated to such spatial encoding is then preserved throughout the coherent mixing period, and subsequently decoded during the course of the data acquisition by the action of a field gradient G_a. This acquisition gradient will unravel the spatial encoding that was created prior to the mixing period and lead to echoes whenever the wavenumber $k = \gamma_a \int_0^t G_a(t') \, dt'$ matches $C\Omega_1$, with C a spatio-temporal ratio under the experimentalist's control. The positions of these "peaks" will thus reflect the usual indirect-domain NMR spectrum. Moreover, oscillating the sign of G_a during the course of the acquisition can undo and redo numerous times such k-encodings, allowing one to monitor the direct-domain Ω_2 frequencies via the t_2-modulations that they will impart on the k/v_1 interferogram. Fourier transformation (FT) of the resulting $S(k/v_1, t_2)$ data set against the direct-domain

* Corresponding author. Fax: +972 8 9344123.
E-mail address: lucio.frydman@weizmann.ac.il (L. Frydman).

acquisition time thus leads to the full 2D $I(v_1, v_2)$ NMR spectrum being sought, from an experiment that can be completed within a single scan.

Fig. 1A illustrates the kind of scanning that the scheme just described will impart onto the spin evolution, on the $(k/v_1, t_2)$-space where the acquisition takes place. This Figure—which assumes that G_a is being subject to a square-wave modulation of period $2T_a$ but would not change in essence if other types of modulations were used [8]—highlights one of the main complications encountered upon processing the ultrafast 2D NMR data. It shows that points in this experiment are laid out in a zig-zagging trajectory associated to the application of positive and negative acquisition gradients, which is not a regular distribution readily amenable to FT along the direct t_2 domain. Indeed, extracting a t_2 data vector along an arbitrary k-value reveals that points are not arranged in a uniform fashion, and that while data collected under the action of either the positive or the negative gradients are spaced by periods $2T_a$, both data sets are shifted from one another by a delay $0 \leqslant \tau(k) \leqslant 2T_a$ depending on the particular k-value associated to the vector (Fig. 1B). Therefore, except for the pathological vectors located at $k = 0$,
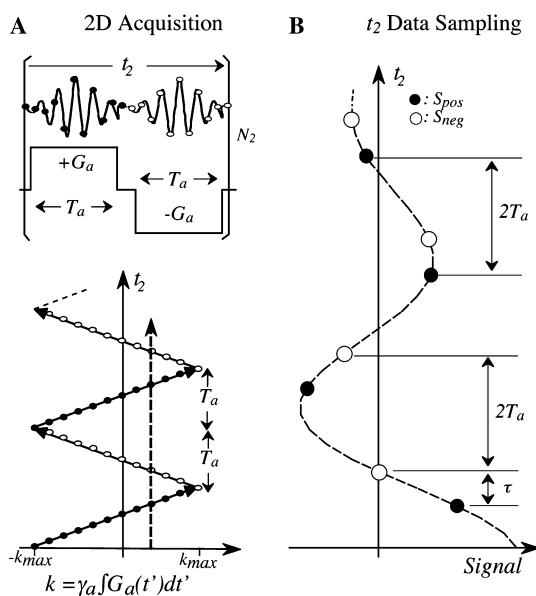

Fig. 1. (A) Schematic representation of how digitized points in ultrafast 2D NMR appear distributed throughout the $(k/v_1, t_2)$ acquisition space. Closed and open dots symbolize the coordinates of points digitized during the course of the $+G_a$ and $-G_a$ acquisition gradients; T_a is the duration over which each of these gradients is applied. Due to the uneven distribution with which points are spread, "conventional" ultrafast processing sorts data out into independent "positive" (●) and "negative" (○) sets that are then individually FT. Both 2D data sets can then be co-added for the sake of improving the overall S/N. (B) Representation of an arbitrary $S_k(t_2)$ FID extracted from (A) at the position of the dashed arrow, showing the definition of the τ delay involved in the interlaced FT processing; Eq. (1).

$\pm k_{max}$, data collected under the action of positive and negative gradients cannot be jointly Fourier transformed against t_2. To deal with this complication we have been hitherto processing ultrafast 2D NMR data sets separately; i.e., rearranging the data string collected by the spectrometer into *two* 2D interferograms $S_{pos}(k/v_1, t_2)$ and $S_{neg}(k/v_1, t_2)$ associated with the action of the positive and the negative gradients, FT-ing each one of these regular grids of data separately against their respective acquisition times t_2, and if need be co-adding the two resulting spectra $I_{pos}(k/v_1, v_2)$ and $I_{neg}(k/v_1, v_2)$ into a single spectral data set. When executed with care this latter step is liable to increase the overall signal-to-noise ratio (S/N), even if instrumental problems sometimes prevent this gain from reaching the full $\sqrt{2}$ theoretical enhancement. In several instances we have consequently refrained from carrying out such recombination, and our current "conventional" approach to ultrafast 2D data processing focuses only on one of these sets.

As a result of such relatively inefficient mode of processing the experimental data, dual sensitivity losses are inflicted: S/N is degraded by a factor of $\sqrt{2}$ due to the fact that only half the signal is employed in the FT, while the effective dwell time Δt_2 along the direct domain becomes effectively twice its potential minimum: $2T_a$ instead of T_a. This latter aspect means that in order to cover specific direct- and indirect-domain bandwidths $SW_2 = (\Delta t_2)^{-1}$ and $SW_1 = \gamma_a G_a \Delta t_2 L / t_1^{max}$ (L being the spatial length of the encoding) the effective acquisition gradient will also have to be doubled, leading to a need for an increased receiver bandwidth—given in all cases by a lower bound of $\gamma_a G_a L$ [9]—and thereby to an additional $\sqrt{2}$ noise magnification. On the other hand, if it were possible to combine both "positive" and "negative" data sets into a single processing operation along t_2, the doubling of the data points coupled to the reduction of the effective dwell time Δt_2 would simultaneously alleviate both problems. Fortunately, a simple procedure has been described in the literature capable of dealing exactly with the kind of data distribution arising in ultrafast 2D NMR experiments along t_2: the interlaced FT [10]. This reconstruction scheme, which has been demonstrated in a variety of MRI settings involving 2D FT's [11,12], is meant to process two arrays of data points whose individual spacing is given by identical increments Δt_2, but which are shifted from each other by an interval $\tau \neq \Delta t_2/2$. As can be appreciated from Fig. 1B this is exactly the kind of scenario arising along t_2 in ultrafast 2D NMR for every value of k except for pathological rows located at the $\pm k_{max}$ edges, where no information in-between $2T_a$ intervals is available. For all remaining k-values two simple linear combinations of the $\{I_{pos}(k/v_1, v_2), I_{neg}(k/v_1, v_2)\}$ spectra arising from the fast FT of "positive" and "negative" data arrays

$$G(k/v_1, v_2) = -\frac{\exp[-i \cdot sg(v_2)\pi\tau/T_a]}{1 - \exp[-i \cdot sg(v_2)\pi\tau/T_a]} I_{pos}(k/v_1, v_2)$$
$$+ \frac{\exp[-i2\pi\tau v_2]}{1 - \exp[-i \cdot sg(v_2)\pi\tau/T_a]} I_{neg}(k/v_1, v_2),$$

(1a)

$$H(k/v_1, v_2) = \frac{1}{1 - \exp[-i \cdot sg(v_2)\pi\tau/T_a]} I_{pos}(k/v_1, v_2)$$
$$- \frac{\exp[-i2\pi\tau v_2]}{1 - \exp[-i \cdot sg(v_2)\pi\tau/T_a]} I_{neg}(k/v_1, v_2),$$

(1b)

provide an intermediate stage from where to characterize the direct-domain spectrum over the full $SW_2 = 1/T_a$ range while coherently adding both sets of signals. Indeed, a total 2D $I(k/v_1, v_2)$ spectrum over this spectral range can be reconstructed from the G, H functions in Eq. (1) as

$$I(k/v_1, v_2) = \begin{cases} H(k/v_1, v_2 + \frac{1}{2T_a}), & -\frac{1}{2T_a} \leqslant v_2 \leqslant -\frac{1}{4T_a}, \\ G(k/v_1, v_2), & -\frac{1}{4T_a} \leqslant v_2 \leqslant +\frac{1}{4T_a}, \\ H(k/v_1, v_2 - \frac{1}{2T_a}), & +\frac{1}{4T_a} \leqslant v_2 \leqslant +\frac{1}{2T_a}. \end{cases}$$

(2)

The principles whereby these combinations succeed in unraveling the spectral data have been dealt with elsewhere [10–12] and hence will not be here re-derived; suffice it to say that Eqs. (1) involve a de-aliasing procedure whereby the delay τ between the two sets is employed to distinguish and cancel out signals whose $|v_2|$ precession frequencies where smaller than $1/(4T_a)$, from those oscillating in the $1/(4T_a) \leqslant |v_2| \leqslant 1/(2T_a)$ interval. Frequencies outside the $[+1/(2T_a), -1/(2T_a)]$ bound will be subject to fold over, according to a behavior that differs from that of the usual FT.

To explore the potential usefulness of the interlaced FT in ultrafast 2D NMR, a series of experiments were assayed. A Varian iNova500 instrument equipped with an inverse 5 mm probehead and triple-axis gradients was used, and acquisitions relying on the continuous encoding sequences described elsewhere [13] were executed. The data resulting from these experiments were then processed in two different manners: a "conventional" way whereby data were separated into $S_{pos}(k/v_1, t_2)$ and $S_{neg}(k/v_1, t_2)$ sets and then only one of these is processed into a spectrum, and the new interlaced FT way whereby the processing of the individual sets was
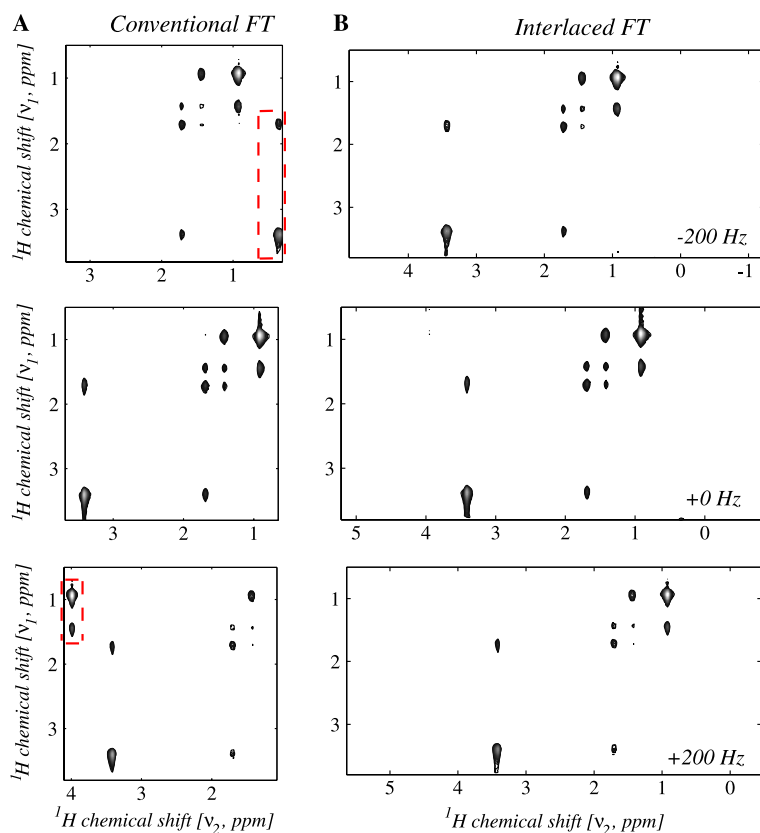

Fig. 2. Single-scan 2D ^{1}H NMR spectra acquired on an *n*-butylchloride/CDCl$_3$ sample as a function of the indicated receiver offsets, and subsequently processed using the conventional (A) and the interlaced (B) FT algorithms. In all cases the TOCSY sequence described in [13] was employed with the following parameters: G_e = 10 G/cm, chirped pulse bandwidth = 79 kHz, t_1^{max} = 50 ms, G_a = 28 G/cm, N_2 = 80, T_a = 0.29 ms sampled with a constant dwell of 2 μs and followed by a 20 μs gradient switching delay, and a 20 ms DIPSI-2 mixing pattern. As throughout the rest of the paper 2D plots are plotted at a constant per parts per million length, and contours are illustrated in magnitude mode using a 10% threshold. Marked on the left-hand column inside the dashed-boxes are 2D peaks undergoing folding due to the limited SW_2 afforded by the conventional processing mode.

followed by the rearrangements summarized in Eqs. (1) and (2). Except for the different treatments of the data along v_2 both processing procedures are in fact fairly similar; they both require rearranging the experimental data into their appropriate $(k/v_1, t_2)$ coordinates, shearing the resulting data interactively so as to compensate for potential $\pm G_a$ gradient imbalances, potentially zero-filling and weighting the data, and executing a series of fast FTs. Besides the calculations given in Eqs. (1) and (2) the only actual extra precaution required by the interlaced as opposed to the conventional processing, concerns ensuring a proper alignment of the indirect-domain k-peaks appearing in both "positive" and "negative" data sets. For the conditions employed in the present study this could be easily achieved simply by left shifting ca. 20 μs worth of data from the original experimental FID—presumably a procedure needed to account for certain propagation delays during the course of the acquisition. Accounting for the dead times involved in the $\pm G_a$ gradient switching occurring during the data acquisition was also found important, as these in turn become part of the $\tau(k)$ delays appearing in Eq. (1). This action, as well as all the remaining numerical

and graphical procedures implemented in this study, were carried out with the aid of software packages custom-written with Matlab 6.5 (The MathWorks Inc.).

A first example of the potential associated with the interlaced FT is shown in Fig. 2, which compares a series of single-scan 2D TOCSY ^{1}H NMR plots recorded on an n-butylchloride/CDCl$_3$ solution, as a function of the receiver carrier frequency defining the center of the spectrum along v_2. Spectral windows throughout these experiments were chosen so as to fit the complete TOCSY correlation even when executing a conventional processing of the data. This of course, provided that the radiofrequency carrier is properly centered. When this condition is not accurately met folding of the peaks becomes clearly evident upon relying on the conventional data processing, whereas the SW_2 doubling afforded by the interlaced FT prevents this from happening over a wider range of offsets. Another example of the improvements brought about by this new way of processing is illustrated in Fig. 3, which shows single-scan 2D TOCSY NMR spectra recorded on the n-butylchloride as well as on a 5 mM tyrosine ethylester/CDCl$_3$ solution, under acquisition conditions that do not pro-
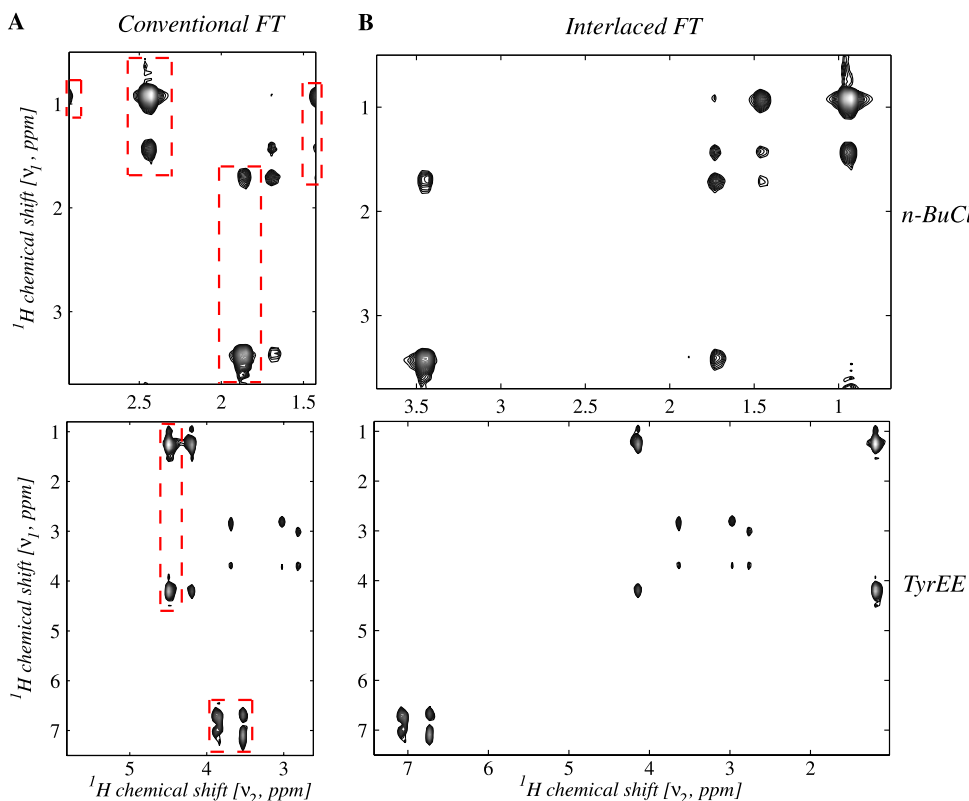

Fig. 3. Single-scan 2D ^{1}H TOCSY NMR spectra acquired on n-butylchloride/CDCl$_3$ (top) and tyrosine ethylester/CDCl$_3$ (bottom) samples, under conditions where the conventional processing is unable to deliver the full necessary spectral width along the direct domain. Notice how the folded patterns included in the dashed boxes after conventional processing (A) are unfolded upon processing the experimental data using the interlaced FT (B). Main acquisition parameters in these experiments were as follows. (Top) $G_e = 10$ G/cm, chirped pulse bandwidth = 79 kHz, $t_1^{max} = 50$ ms, $G_a = 13$ G/cm, $N_2 = 40$, $T_a = 0.604$ ms ($SW_1 = 1600$ Hz), 20 ms DIPSI-2 mixing. (Bottom) $G_e = 10$ G/cm, chirped pulse bandwidth = 79 kHz, $t_1^{max} = 15$ ms, $G_a = 21$ G/cm, $N_2 = 64$, $T_a = 0.272$ ms ($SW_1 = 3800$ Hz), 30 ms DIPSI-2 mixing.

vide a large enough spectral window to fit all the peaks upon conventional processing. As can be appreciated in this Figure's right-hand side, combining $S_{\text{pos}}(k/v_1, t_2)$ and $S_{\text{neg}}(k/v_1, t_2)$ via the interlaced FT yields 2D spectra that are entirely fold-free at no additional costs in terms of the experimental setup.

Setting up the ca. 6.5 ppm wide spectral windows required to fit all the ^{1}H peaks in tyrosine ethylester's ultrafast ^{1}H 2D NMR spectrum, is somewhat of a challenge when relying on the conventional data processing mode. In the 500 MHz instrument employed this implied applying a decoding gradient $G_a > 48$ G/cm (out of a maximum of ≈ 60 G/cm) during the course of the acquisition. The single-scan 2D ^{1}H TOCSY spectrum then obtained in this fashion is presented in Fig. 4, and compared with the one achievable for similar SW_2 conditions using the interlaced FT. This comparison illustrates well the three main practical benefits resulting from the new processing procedure. First, it shows that

the ability of the interlaced FT to accommodate T_a times that are over twice as long (the extra gain given by the dead times associated to the gradient switching) implies that gradients are cut by a factor $\geqslant 2$ and the effective powers delivered into the gradient assembly become considerably smaller—in the present case by a factor of 5 vis-à-vis the powers associated with an experiment employing the conventional processing. This is an important consideration when limited by gradient hardware considerations. A second hardware-related benefit afforded by the interlaced FT concerns the improvement that can be noticed along the indirect spectral domain of Fig. 4B in terms of the peaks' line widths. This enhanced resolution stems from the fact that even when maximum digitization rates are used (in the present instrument corresponding to 500 kHz) the definition of the echoes making up the peaks along the k/v_1 dimension becomes compromised when employing the short T_a times demanded by the conventional processing for
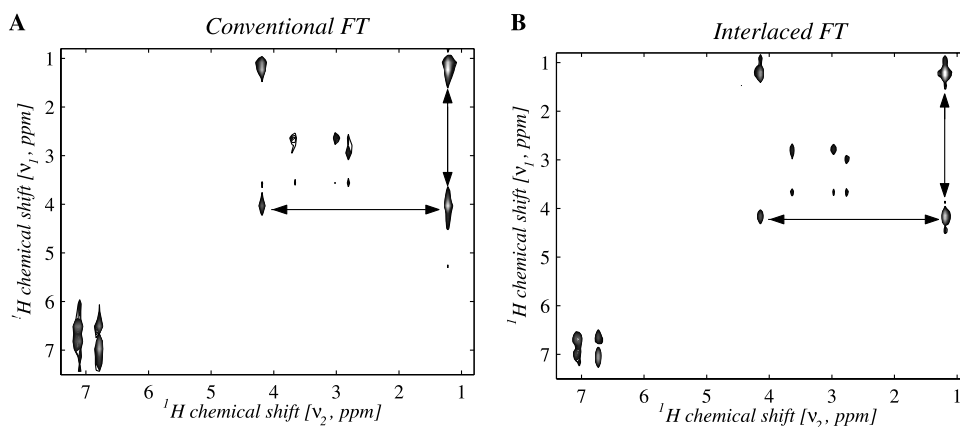

Fig. 4. Comparison between single-scan 2D ^{1}H TOCSY NMR spectra acquired on tyrosine ethylester/CDCl$_3$ under conditions leading to fully unfolded spectra after using a conventional (A) and an interlaced (B) FT of the data along t_2. The spectrum in (B) was collected under the conditions listed for Fig. 3B; the acquisition conditions in (A) were similar except for and increase in G_a from 21 to 48.3 G/cm, and a decrease in T_a from 0.272 to 0.11 ms to fit the full $SW_2 = 3333$ Hz window. The increase in G_a implied that bigger analog receiving filter bandwidths had to be employed, 190 kHz in (A) vs 84 kHz in (B); also longer gradient switching dead times (40 μs instead of 20 μs) became necessary. The arrows indicate the positions of the cross-sections displayed in Fig. 5.
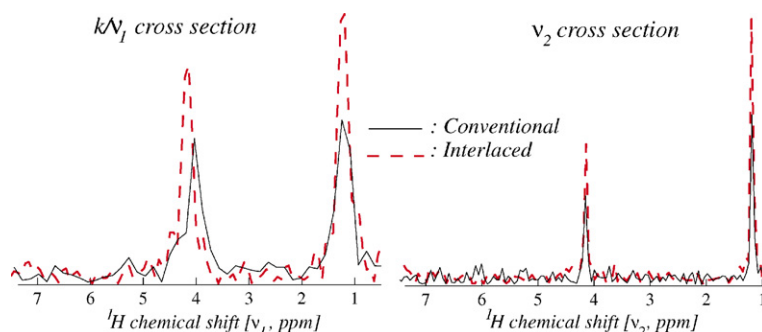

Fig. 5. Comparison between cross-sections extracted from the single-scan results presented in Fig. 4, at the positions indicated by the arrows in the conventional and in the interlaced 2D NMR plots. Average sensitivity gains measured for peaks subject to the interlaced vis-à-vis a conventional FT was 80% when considering the k/v_1 cross-section, and 110% when considering the v_2 trace. The slight shifts observed in the peak positions along the indirect domain are likely a consequence of non-idealities in the gradient's behavior.

SW_1, $SW_2 \geqslant 6$ ppm. This limitation is lifted upon using the longer T_a's required by the interlaced FT. Finally, the third and most important benefit resulting from the use of the new processing method concerns the improvement observed in the overall spectral S/N. This is highlighted by the various cross-sections compared in Fig. 5, extracted from the 2D spectra shown in Fig. 4 at selected k/v_1 and v_2 values. Theory predicts that except

when dealing with very small values of τ, where the numerators and denominators in Eq. (1) become ill-defined and the conditions required by the joint processing are not met, the sensitivity of the interlaced FT spectrum should exceed that of its conventional counterpart by a factor of ≈ 2: a $\sqrt{2}$ enhancement arising from doubling the number of t_2 data involved, and another $\sqrt{2}$ enhancement arising from a noise-defining filter band-
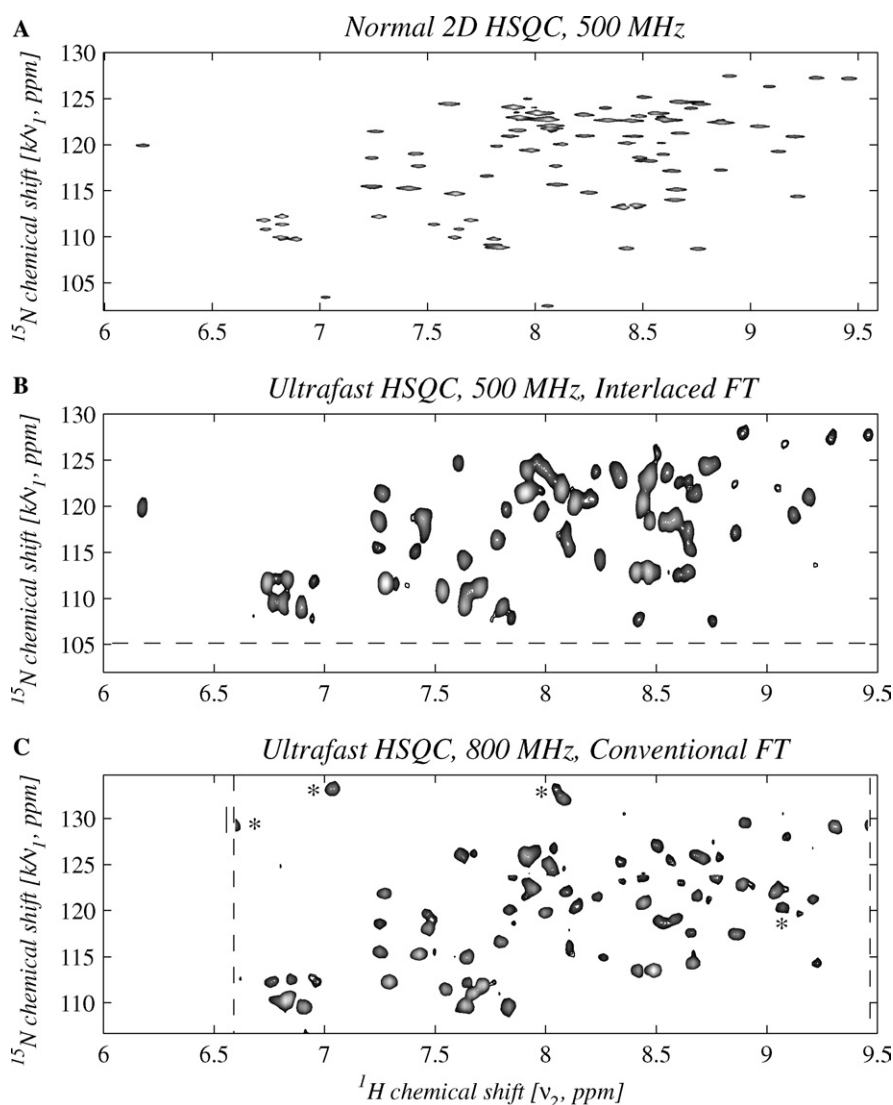

Fig. 6. Comparison between: (A) A normal 2D ^{1}H–^{15}N HSQC 500 MHz NMR spectrum acquired on [U-^{15}N]ubiquitin arising from the acquisition of 250 t_1 increments, each of them involving eight phase-cycled scans (plus 4 dummy scans), sampled with 1024 points along t_2 and separated by a 5 s recycle delay ($t_1^{max} = 100$ ms, $t_2^{max} = 128$ ms, and total acquisition time $\approx$4 h). (B) An ultrafast 2D HSQC NMR experiment processed on the basis of the interlaced FT, involving the same spectrometer and sample but relying on only four phase-cycled single-scan 2D acquisitions. (C) An analogous four-scan ultrafast 2D HSQC acquisition, but at a higher field and relying on a conventional FT processing of "positive" and "negative" data sets followed by their subsequent co-addition. All spectra were collected on the same His-tagged 3.2 mM protein sample dissolved in 90/10% H_2O/D_2O at 25 °C, employing a Watergate suppression of the solvent signal prior to the data acquisition. The ultrafast 2D HSQC experiment in (B) was collected at 500 MHz using a continuous spatial encoding defined by $G_e = 40$ G/cm and $t_1^{max} = 20$ ms, and a spatial decoding given by $G_a = 5.6$ G/cm, $N_2 = 48$, $T_a = 0.47$ ms sampled with a physical dwell of 2 μs and followed by 64 μs dead times for the sake of gradient switching and {^{15}N}-decoupling, and a 20 kHz filter bandwidth. The spectrum in (C) was collected on an 800 MHz Bruker Avance NMR spectrometer and arose from a discrete 16-pulse excitation with $G_e = 51$ G/cm and $t_1^{max} = 14$ ms, and a decoding given by $G_a = 22.2$ G/cm, $N_2 = 64$, $T_a = 0.10$ ms plus a 106 μs dead time for gradient switching and decoupling, 2 μs physical sample dwells, and a 125 kHz filter bandwidth. Dashed lines in (B) and (C) indicate the actual limits of the spectral windows acquired; asterisks in (C) denote folded resonances.

width that can now be cut by approximately half. A quantitative comparison of the cross-sections shown in Fig. 5 shows that this expectation is experimentally fulfilled. The cross-sections also illustrate the absence of artificial peak sidebands spaced by $\pm SW_2/2$ along the v_2 axes—which is the most commonly observed artifact in the presence of any imbalances between $S_{pos}(k/v_1, t_2)$ and $S_{neg}(k/v_1, t_2)$.

The use of the interlaced FT pertains only the data processing stage of ultrafast NMR, and can thus be applied regardless of the kind of 2D experiment involved. As an illustration of this we present in Fig. 6 a heteronuclear example, where ultrafast ^1H–^{15}N 500 MHz HSQC data recorded on a 3.2 mM ^{15}N-labeled ubiquitin sample were processed via the interlaced FT. To give a perspective on the enhanced sensitivity delivered by this procedure we compare these data with a set collected on the same sample on an 800 MHz NMR instrument (Fig. 6C) within the same number of scans but using a "conventional" processing. Whereas using this higher field affords a resolution enhancement, it is interesting to note that the sensitivity displayed by the interlaced FT 500 MHz spectrum is similar to (if not higher than) the one obtained in the higher field machine. While the overall demands made on the experiment become actually eased. And of course, in either case a comparison with a 2D spectrum collected in the traditional multiscan fashion (Fig. 6A) yields an immediate identification of the various sites in the protein.

We believe that biomolecular 2D NMR acquisitions such as the one just illustrated, where S/N is at a premium, might become one of the main driving forces behind the use of the interlaced FT. In fact this procedure becomes particularly stable for heteronuclear cases like the one in Fig. 6, where the need to insert $(\pi)_N$ pulses in-between $\pm G_a$ periods for the sake of achieving heteronuclear decoupling puts a serious constraint to the minimal duration that dwell times $2T_a$ along t_2 may take ($\geqslant 70$–80 μs), while automatically lifting the limitations facing interlaced FT at the $\pm k_{max}$ coordinates. Higher-dimensional ultrafast NMR [7], where the penalties associated to separating data along the lines described in Fig. 1 are even costlier than in 2D experiments, are also envisioned as important beneficiaries of this procedure. So are potential in vivo investigations. Last but not least it is also worth remarking that the full sensitivity gains associated to the interlaced FT can only be reaped whenever the noise-determining receiver bandwidth can be optimally adjusted according to $\gamma_a G_a L$ regardless of the data digitization rate used; not all major spectrometer manufacturers currently offer such a capability.

References

[1] J. Jeener. Lecture presented at Ampere International Summer School II, Basko Polje, Yugoslavia, September 1971.
[2] W.P. Aue, E. Bartholdi, R.R. Ernst, Two dimensional spectroscopy. Application to nuclear magnetic resonance, J. Chem. Phys. 64 (1976) 2229–2246.
[3] R.R. Ernst, G. Bodenhausen, A. Wokaun, Principles of Nuclear Magnetic Resonance in One and Two Dimensions, Clarendon, Oxford, 1987.
[4] H. Kessler, M. Gehrke, C. Griesinger, Two-dimensional NMR spectroscopy: Background and overview of the experiments, Angew. Chem. Int. Ed. Engl. 27 (1988) 490–536.
[5] L. Frydman, T. Scherf, A. Lupulescu, The acquisition of multidimensional NMR spectra within a single scan, Proc. Natl. Acad. Sci. USA 99 (2002) 15858–15862.
[6] L. Frydman, A. Lupulescu, T. Scherf, Principles and features of single-scan two-dimensional NMR spectroscopy, J. Am. Chem. Soc. 125 (2003) 9204–9217.
[7] Y. Shrot, L. Frydman, Single-scan NMR spectroscopy at arbitrary dimensions, J. Am. Chem. Soc. 125 (2003) 11385–11396.
[8] N. Sela, H. Degani, L. Frydman, Ultrafast 2D NMR spectroscopy using sinusoidal gradients: Principles and ex-vivo brain investigations, Magn. Reson. Med. 52 (2004) 893–897.
[9] B. Shapira, A. Lupulescu, Y. Shrot, L. Frydman, Line shape considerations in ultrafast 2D NMR, J. Magn. Reson. 166 (2004) 152–164.
[10] R.N. Bracewell, The Fourier Transform and its Applications, McGraw-Hill, New York, 1978 (Chapter 10).
[11] K. Sekihara, H. Kohno, New reconstruction technique for echo planar imaging to allow combined use of odd and even numbered echoes, Magn. Reson. Med. 5 (1987) 485–491.
[12] G. Metzger, X. Hu, Application of interlaced fourier transform to echo-planar spectroscopic imaging, J. Magn. Reson. 125 (1997) 166–170.
[13] Y. Shrot, B. Shapira, L. Frydman, Ultrafast 2D NMR spectroscopy using a continuous spatial encoding of the spin interactions, J. Magn. Reson. 171 (2004) 162–169.